REGIONALITY OF DUST STORM EXPANSION ON MARS.

K. Ogohara, *Japan Aerospace Exploration Agency, Institute of Space and Astronautical Science, Kanagawa, Japan (ogohara.kazunori@jaxa.jp)***, T. Satomura,** *Division of Earth and Planetary Science, Kyoto University, Kyoto, Japan***.**

Introduction

Dust storms of several scales have been observed so far. According to the definition of dust storms by *Cantor et al.* (2001), local dust storms were defined as dust storms whose size is smaller than 1.6×10^6km^2 and duration is shorter than 2 sols. Regional dust storms were defined as dust storms whose size is larger than 1.6×10^6km^2 and duration is longer than 2 sols. However, the three dimensional structures, lifetimes and expansion mechanisms of these dust storms have not been understood because of low time and spacial resolutions of past observations by polar orbital satellites. In this study, we attempt to investigate mechanisms of dust storm development into regional and global dust storms using numerical simulations.

Approach

Figure 1 shows locations of local dust storms and the centers of regional dust storms on Mars. Many of local dust storms occur near large topographies and the polar cap edges. However, the centers of regional dust storms do not always coincide with areas where many local dust storms are observed. This fact means that local dust storms can not develop in some regions. In our opinion, one likely explanation is that there are favorable regions for expansion of dust storms on Mars (denoted as FRs hereinafter) associated with synoptic or larger scale atmospheric phenomena, i.e., dust storms that enter an FR can develop into larger storms and dust storms that do not enter an FR do not develop into larger storms. Thus, we take the following approach to meteorologically clarifying the development mechanisms of regional dust storms with numerical simulations.

1 Preparation of global maps of dust expansibility that indicate the locations of FRs on Mars.

2 Meteorological investigation of why the identified FRs are favorable for the expansion of dust.

In this study, we describe preparation of global maps of dust expansibility.

Model and Experimental setup

A general circulation model (GCM) used in this study is based on a sigma–coordinate primitive model used by *Ogohara and Satomura* (2008). *Ogohara and Satomura*

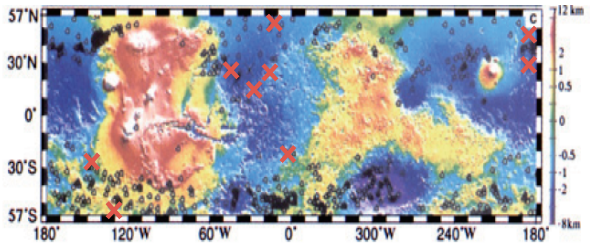

Figure 1: Locations of local dust storms from 1999 through 2000 (black dots). Red crosses indicate the centers of regional dust storms. Plate 1 presented by *Cantor et al.* (2001) is modified.

(2008) used the dust mixing ratio q as a prognostic variable in regards to dust. A serious shortcoming of the prognostic equation for q is that, when the prognostic equation is discretized, the globally integrated total dust mass becomes non-conservative with integration over time, even if the surface dust flux is zero. Therefore, based on an equation for water vapor used by *Allen et al.* (1991), we introduce the following equation as a prognostic equation of dust:

$$\frac{\partial p_s q}{\partial t} = -\frac{1}{a(1-\mu^2)}\frac{\partial (p_s q U)}{\partial \lambda} - \frac{1}{a}\frac{\partial (p_s q V)}{\partial \mu} - \frac{\partial (p_s q \dot{\sigma})}{\partial \sigma} + S_{src}(\lambda,\phi,\sigma) + S_{phys}(\lambda,\phi,\sigma). \quad (1)$$

Meaning of the variables are described in Appendix.

If equation (1) is calculated using the spectral method, the Gibbs phenomenon around localized dust would be inevitable. In order to avoid such unrealistic dust transportation, we calculate $p_s q$ in the finite difference scheme using modeled winds derived from the spectral part of the model. We use a 1D cell-integrated semi-Lagrangian scheme (CISL) (*Nair and Machenhauer*, 2002) for the longitudinal and latitudinal advection of dust and the second-order van-Leer scheme (*van Leer*, 1977) for the vertical advection of dust. Near the poles, however, dust advection in all directions is calculated by the van-Leer scheme. A flux limiter (*Collela and Woodward*, 1984) is used to ensure that these advection schemes are monotonic and positive-definite.

The atmospheric mass change due to CO_2 condensation and sublimation largely modifies the meridional wind near the surface around the polar cap edges (*Ogohara and Satomura*, 2010). Therefore, we introduce a surface pressure change representing the atmospheric

mass change due to the CO_2 phase-change into our Martian GCM. This surface pressure change and the seasonal variation of the ice caps are given by the deposited CO_2 ice layer data in the Mars Climate Database (http://johnson.lmd.jussieu.fr:8080/las/servlets/dataset). The atmospheric temperature is adjusted to the condensation temperature of CO_2 when the temperature falls below the condensation temperature.

In order to find regions that are favorable for dust storm expansion, we inject a certain amount of dust into the atmosphere at 576 sources over the planet and compare regions in which the injected dust spreads. The locations of the centers of the dust sources are indicated by the small black dots shown in Figure 2. In one run, dust is continuously injected into the atmosphere from only one dust source for 1 sol. In another run, dust is injected from another source for 1 sol. This means that 576 independent runs, in which dust is injected from one of 576 different sources, are performed. The period of dust injection, 1 sol, is the maximum duration of local dust storms as defined by *Cantor et al.* (2001). The rate of dust injection is 2.0×10^5 kg s^{-1}, the time integral of which gives an approximation of the mean dust loading of the regional dust storms reported by *Cantor et al.* (2001). We also perform a control run in which dust is not injected. We do not account for spontaneous dust loading from the surface depending on surface wind stress.

Dust injection is expressed as a source term of $p_s q$, namely, $S_{src}(\lambda,\phi,\sigma)$, in equation (1) instead of the surface dust flux. In the present study, $S_{src}(\lambda,\phi,\sigma)$ is given at each time step as follows:

$$S_{src}(\lambda,\varphi,\sigma) = \begin{cases} \dfrac{p_s C}{1-B_{top}(\lambda,\varphi)}\left[\dfrac{1}{2}\left\{(1+\cos(\dfrac{\pi r}{r_0})\right\}\right]^{0.6} & \left(\begin{array}{l} r<r_0, \\ \sigma > B_{top} \end{array}\right. \\ 0 & \text{elsewhere.} \end{cases}, \quad (2)$$

where r is the great-circle distance from the center of a dust source. The radius of the dust source, r_0=(1/16)πa, is comparable with the horizontal scale of large local dust storms as defined by *Cantor et al.* (2001). The sigma coordinate at the top of a dust source, $B_{top}(\lambda,\phi)$, is defined later herein. The columnar dust mass of injected dust is large near the center of the dust source. C is a constant in the range of $B_{top}(\lambda,\phi) < \sigma < 1$ and satisfies the following:

$$a^2 \int_{-\frac{\pi}{2}}^{\frac{\pi}{2}} \int_0^{2\pi} \int_{B_{top}(\lambda,\varphi)}^{1} S_{src}(\lambda,\varphi,\sigma) d\sigma \sin\varphi d\lambda d\varphi = 2.0\times10^5 g, \quad (3)$$

where g is the gravitational acceleration. This is because the rate of dust injection is 2.0×10^5 kg s^{-1}.

$B_{top}(\lambda,\phi)$ in equations (2) and (3) is determined based on *Takemura et al.* (2000). In the Martian atmosphere, dust is expected to be mixed vertically in the mixing layer for the case in which dust is loaded during the day. On the other hand, dust is expected to remain in the inversion layer for the case in which dust is loaded during the night. Thus, denoting the surface potential temperature as θ_s, dust is injected into the layer for which the potential temperature θ is lower than θ_s+$\delta\theta$. $B_{top}(\lambda,\phi)$ is the sigma coordinate that satisfies the following:

$$\theta(\lambda,\varphi,B_{top}(\lambda,\varphi)) = \theta_s(\lambda,\varphi) + \delta\theta. \quad (4)$$

$B_{top}(\lambda,\phi)$ is the sigma coordinate of the lowest layer if the potential temperature of the lowest layer is higher than θ_s+$\delta\theta$ inside the nocturnal inversion layer. $\delta\theta$ is 3 K here while *Takemura et al.* (2000) used $\delta\theta = 0$ K.

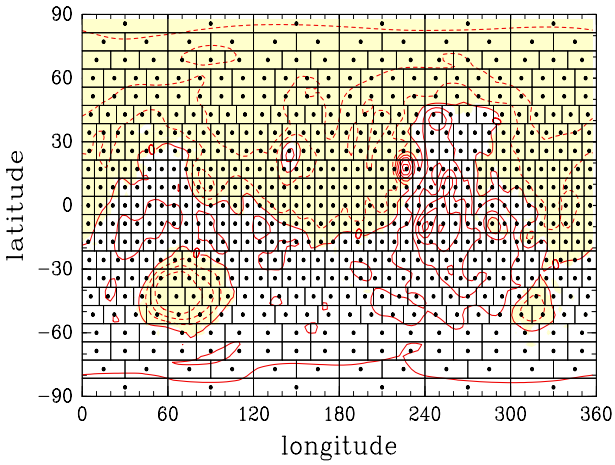

Figure 2: A distribution of dust sources used in out simulations. Centers of dust sources are located on black dots. Red lines indicate Martian topography. The contour interval is 2000 m. Solid and dotted lines indicate positive and negative altitudes, respectively.

Results

Injected dust cannot be distinguished from the background dust in our model. Therefore, we must first define a region obscured by injected dust. In the present study, we define this region as a region in which the columnar dust mass is at least 0.002 kg m^{-2} larger than that in the control case. This value 0.002 kg m^{-2} corresponds to a dust optical depth (5–11.6 μm) of approximately 0.07 and is sufficiently large as a dust storm criterion (Fig. 2 presented by *Smith et al.* (2002)). Such a two-dimensional definition of a dust storm area is used in the next section.

In Figure 3, area obscured by injected dust in each dust source indicated in Figure 2 is shown by colors. Figure 3 indicates where dust tends to expand on Mars in

the northern fall and visualizes locations of FRs. Dust injected near Tharsis, the Sirenum–Aonia region and Acidalia Planitia is transported extensively 1 sol after the start of the dust injection. On the other hand, dust injected inside the Hellas basin and near the Margaritifer Terra does not expand extensively. Dust injected from the east of Erisyum Mons and Arabia Terra is also transported extensively 2 sols after the start of the dust injection. However, dust injected from the Hellas basin and the Margaritifer Terra remains localized around the source areas even 2 sols after the start of the dust injection. Dust injected from highlands can be transported upward and easily expand extensively because dust is radiatively active in the model. A mid-latitudes jet and high baroclinicity result in the strong vertical shear of zonal wind and strong baroclinic waves in the mid-latitudes. These are also key phenomena for dust storm expansion around the FRs. We prepare another global maps for the cases in which dust starts to be injected 12 hours after the dust injection start of the above run (not shown). As a result, dust expansibility around the Sirenum–Aonia region and Tharsis decreases and that around the Acidalia–Utopia region increases. This result shows that the diurnal phenomena are important for dust storm expansion in these regions.

Future work

Results of the northern fall simulations in certain year have been shown in this study. Multi-year simulations are necessary for climatological investigation of dust expansibility. FRs found in results of such multi-year simulations in the future are clues to understanding mechanisms of dust storm expansion climatologically on Mars.

Appendix:Variables in equation (1)

$$\dot{\sigma} \equiv \frac{d\sigma}{dt}$$
$$\mu \equiv \sin\varphi$$
$$U \equiv u\cos\varphi$$
$$V \equiv v\cos\varphi$$

p_s:surface pressure, ϕ:latitude, λ:longitude, σ:σ coordinate, a:Mars radius, S_{phys}:changes due to physical processes, S_{src}:source term of $p_s q$.

References

[1] Allen, D. J., A. R. Douglass, R. B. Rood, and P. D. Guthrie (1991), Application of a monotonic upstream-biased transport scheme to three-dimensional constituent transport calculations, Mon. Wea. Rev., 119, 2456–2464.

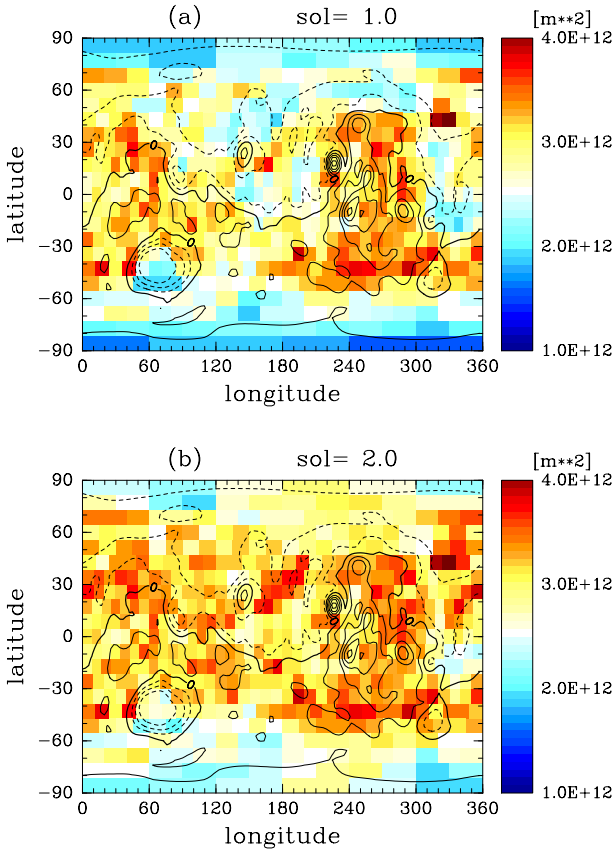

Figure 3: Maps showing how widely dust injected from the dust sources shown in Figure 2 is transported. The colored boxes indicate the locations of dust sources. The colors of the boxes indicate the maximum area of the region obscured by dust injected from the dust source (a) 1 sol or (b) 2 sols after the end of dust injection. Red regions indicate FRs. Thin solid, thick solid, and thin dashed black contour lines indicate the same topography as in Figure 2.

[2] Cantor, B. A., P. B. James, M. Caplinger, and M. J. Wolff (2001), Martian dust storm: 1999 Mars Orbiter Camera observations, J. Geophys. Res., 106(E10), 23653–23687.

[3] Colella, P., and P. R. Woodward (1984), Piecewise parabolic method for gas-dynamics simulations, J. Comput. Phys., 54, 174–201.

[4] Nair, R. D., and B. Machenhauer (2002), The mass-conservative cell-integrated semi-Lagrangian advection scheme on the sphere, Mon. Wea. Rev., 130, 649–667.

[5] Ogohara, K., and T. Satomura (2008), Northward movement of Martian dust localized in the region of the Hellas Basin, Geo. Res. Lett., 35, L13201, doi:10.1029/2008GL034546.

[6] Ogohara, K., and T. Satomura (2010), Changes in mass flow caused by CO_2 condensation in the Martian atmosphere, Adv. in Geosci., 19, 195–205.

[7] Smith, M. D., B. J. Conrath, J. C. Pearl, and P. R. Christensen (2002), Thermal Emission Spectrometer observations of Martian planet-encircling dust storm 2001A, Icarus, 157, 259–263.

[8] Takemura, T., H. Okamoto, Y. Maruyama, A. Numaguti, A. Higurashi, and T. Nakajima (2000), Global three-dimensional simulation of aerosol optical thickness distribution of various origins, J. Geophys. Res., 105(D14), 17853–17873.

[9] van Leer, B. (1977), Toward the ultimate conservative difference scheme. Part IV: A new approach to numerical convection, J. Comp. Phys., 23, 276–299.